

# Gain properties of dye-doped polymer thin films

I. Gozhyk<sup>1,\*</sup>, M. Boudreau<sup>1,5</sup>, H. Rabbani<sup>2</sup>, N. Djellali<sup>1</sup>, S. Forget<sup>2</sup>, S. Chenais<sup>2</sup>, C. Ulysse<sup>3</sup>, A. Brosseau<sup>4</sup>, S. Gauvin<sup>5</sup>, J. Zyss<sup>1</sup>, and M. Lebental<sup>1</sup>

<sup>1</sup> *Laboratoire de Photonique Quantique et Moléculaire, CNRS UMR 8537, Institut d'Alembert FR 3242, Ecole Normale Supérieure de Cachan, 61 avenue du président Wilson, F-94235 Cachan, France.*

<sup>2</sup> *Laboratoire de Physique des Lasers, Université PARIS 13 et CNRS UMR 7538, 99 Avenue Jean-Baptiste Clement, F-93430 Villetaneuse, France.*

<sup>3</sup> *Laboratoire de Photonique et Nanostructures, CNRS UPR20, Route de Nozay, F-91460 Marcoussis, France.*

<sup>4</sup> *Laboratoire de Photophysique et Photochimie Supramoléculaires et Macromoléculaires, CNRS UMR 8531, Institut d'Alembert FR 3242, Ecole Normale Supérieure de Cachan, F-94235 Cachan, France.*

<sup>5</sup> *Groupe de recherche sur les couches minces et la photonique, Département de physique et d'astronomie, Université de Moncton, Moncton, NB, Canada E1A 3E9.*

The demonstration of an electrically pumped organic laser remains a major issue of organic optoelectronics for several decades. Nowadays, hybrid pumping seems a promising compromise where the organic material is optically pumped by an electrically pumped inorganic device on chip. This technical solution requires therefore an optimization of the organic gain medium under optical pumping. Here, we report a detailed study of gain features of dye-doped polymer thin films, in particular we introduce the gain efficiency  $K$ , in order to facilitate comparison between material and experimental conditions. First, we measure the bulk gain by the means of a pump-probe setup, and then present in details several factors which modify the actual gain of the layer, namely the confinement factor, the pump polarization, the molecular anisotropy, and the re-absorption. The usual model to evaluate the gain leads to an overestimation by more than one order of magnitude, which stresses the importance to design the devices according to experimental basis. Then laser thresholds of Fabry-Perot like cavities can be predicted with a very good agreement. Besides, temporal measurements at the picosecond scale are carried out to support the analysis.

PACS numbers: 42.55.Sa, 42.55.Mv, 05.45.Mt, 03.65.Yz, 42.60.Da

## I. INTRODUCTION

Photonic technology based on organic materials has continuously progressed over the last decades. Organic diodes (so-called OLED's) have developed into an industrially viable domain, whereas polymer based integrated optical devices [1–3] have matured into robust alternatives to semiconductor devices. Among their advantages are the possibility for flexible substrates [4], the quasi-unlimited versatility of materials [5], and a more favorable bio- or chemical compatibility [6].

However, for more than twenty years, the direct electrical excitation of stimulated emission in organic semiconductors remains a major challenge [7, 8], although solid-state organic lasers demonstrated their high potential under optical pumping [9, 10]. In fact, electrically-pumped organic material have several losses mechanisms (low electroluminescent efficiency [11], annihilation processes [12, 13], charge-induced absorption [14, 15] and absorption at metal contacts), which grow rapidly with the current [7], creating a negative feedback loop, that results in material degradation at pumping currents far below the threshold value [9][53].

Therefore the excitation of the organic materials via an inorganic electroluminescent pump [12] is now considered as a highly promising approach, since it allows to achieve an *indirect* electrical pumping of the gain medium. Lasing in such hybrid system was successfully demonstrated

under various pumping sources: micro-chip lasers [18], inorganic laser diodes [19, 20], and even incoherent LED's [21]. Indirect electrical excitation requires to revisit optical pumping, since the design of these new type of lasers should account for all the specific features of optically pumped organic materials.

The method proposed in this article aims to facilitate the engineering of photonics devices and provide a tool for material preselection in the framework of electrically driven organic lasers. We introduce herein a systematic description of gain properties, which facilitates the comparison of organic materials. This approach allows also to study the coupling between the spatial modes and the material gain [22]. We stress the crucial influence of the molecular structure and propose a quantitative estimate of the laser threshold depending on the gain. Actually this field has remained largely unexplored, apart from few works on specific concentrations of specific dye molecules [23–26]. For this purpose, our experimental test-beds are dye-doped polymer solid-state lasers based on commercial laser dyes [54], namely DCM, Rhodamine 640 (RH640) and Pyrromethene 605 (PM605), in conventional configurations such as Amplified Spontaneous Emission (ASE) and Fabry-Perot like cavities, see Fig.1. The article is organized as follows. Section II provides a general description of the gain, and introduces the relevant parameters, which are then studied in details in the following Sections. Two complementary techniques to

measure the actual gain of a dye-doped polymer are then demonstrated: in Section III the pump-probe set-up, which measures the gain of a bulk material, and in subsection IV B the Variable Stripe Length (VSL) method, which gives the modal gain, including the geometrical features of a specific device. For comparison, subsection IV A is devoted to the numerical estimation of the gain confinement factor, involved in the definition of the modal gain. Then, based on the measured amplification properties, Sec.V provides a comparison between the experimental laser thresholds and the estimated values. In Sec.VI, the impact of the pump beam polarization on the lasing threshold is accounted for through a model based on the fluorescence anisotropy and is accordingly quantified for the three laser dyes. Spectral features of the micro-lasers are detailed in Section VII. Finally, the different timescales of spontaneous and stimulated emission is evidenced in Section VIII.

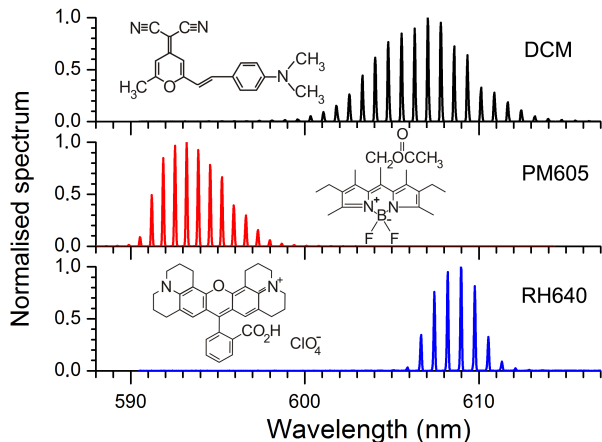


Figure 1: Molecular structures of the laser dyes studied in this article, and normalized emission spectra of the 150  $\mu\text{m}$  Fabry-Perot like micro-laser doped with the corresponding dye.

## II. GAIN IN THIN FILM

Gain properties of active media are of utmost importance for the design of photonic devices. However, usual gain terminology is not appropriate for comparing amplification in different organic materials. In this section, we analyze the commonly used definitions of gain and their limitations, and introduce an alternative way to describe gain in organic thin films.

Two parameters are used in the literature to describe amplification: *material* and *modal* gain. Both describe an average growth rate of electromagnetic flux per unit medium length (in  $\text{cm}^{-1}$  [55]), but in different systems. The *material* gain represents the gain in a bulk, while the *modal* gain describes amplification in the exact thin-film geometry, accounting for transverse overlap of the material gain ( $g_{\text{mat}}$ ) with the pump and propagating mode

profiles ( $\Gamma$ ) inside the layer [27]:

$$g_{\text{mod}} = \Gamma g_{\text{mat}} - \alpha_{\text{mod}} \quad (1)$$

where  $\alpha_{\text{mod}}$  stands for propagation losses.

In the literature, experimental gains are generally obtained in thin-film configuration with the “Variable Stripe Length” technique (VSL) [27]. But, as a matter of fact, these are *modal* gain values and are therefore strongly influenced by the sample geometry (layer thicknesses and refractive indexes), as well as experimental conditions (eg. wavelength and orientation of the pumping beam). Thereby, despite a great number of publications on gain in organic materials, a systematic comparison of gain properties is still lacking due to variations of experimental configurations. It is possible to account for the impact of the system geometry through the estimation of the confinement factor  $\Gamma$ . However, this demands supplementary information, in particular the absorption and stimulated emission spectra of the material under study. An example is provided in Section IV A.

In the framework of electrical pumping, the challenge lies in getting

$$g_{\text{mat}} > 0$$

*A priori*, the gain of the bulk material  $g_{\text{mat}}$  depends on the pump intensity  $I_p$ . Gain in inorganic semiconductors is known to vary logarithmically with the carriers density, which in fact is proportional to the pump intensity, thus leading to:  $g_{\text{mat}} \propto \ln(I_p)$  [28]. However, early works on dye lasers state that amplification in such medium is proportional to the quantity of excited molecules [29], which in its turn depends linearly on the quantity of absorbed photons. This leads to the linear dependance of the gain on pump intensity in an intensity range limited by saturation and non-linear effects:

$$g_{\text{mat}} = K I_p - \alpha_{\text{mat}} \quad (2)$$

where  $\alpha_{\text{mat}}$  represents different kinds of losses:  $\alpha_{\text{mat}} = \alpha_1(I_p) + \alpha_0$ . The losses which depend on the pump intensity  $I_p$  are included into  $\alpha_1$ , like absorption by polarons or by excited states. The other losses, like traps, are represented by  $\alpha_0$ .

The linear coefficient  $K$ , referred hereafter as *gain efficiency*, provides an alternative gain description. We found a confirmation of expression (2) in some publications [16, 25, 26, 30], listing modal gain at several pump intensity values. The inferred gain efficiency  $K$  is about  $10^1$  to  $10^2 \text{ cm.MW}^{-1}$  for dye-doped systems [25, 26] and about  $10^3 \text{ cm.MW}^{-1}$  for conjugated polymers [16]. The unit  $\text{cm.MW}^{-1}$  reveals that we consider the pump intensity and not the pump fluence. This choice will be discussed in Section VIII.

A more comprehensive description of the material gain  $g_{\text{mat}}$  includes spectral influence through the absorption

and emission cross sections  $\sigma_a$  and  $\sigma_e$ :

$$g_{mat} = \sigma_e N^* - \sigma_a N_0 - \alpha_{mat} \quad (3)$$

where all the quantities are considered at the emission wavelength  $\lambda_e$ .  $N^*$  stands for the density of excited molecules, while  $N_0$  for the density of molecules in the ground state. Moreover, gain in laser dyes is homogeneous  $||$ , which means that  $N^*$  does not depend on the wavelength. On the other hand, the spectral dependence of  $\sigma_e$  and  $\sigma_a$  is significant, and the consequences on gain and lasing features are described in Section VII. A comprehensive derivation of both cross sections is presented in Appendix B. While the saturation of absorption remains negligible, expression (2) is a good approximation of Eq. (3). In the next section, this linear dependance is experimentally confirmed in a reasonable range of pump intensity.

In this section, we introduced the gain efficiency  $K$  to describe the amplification properties of the bulk material. It can be measured by pump-probe experiment as illustrated in the next Section. However, the actual gain of a layer is modified by additional parameters: the confinement factor  $\Gamma$  (Sec. IV), the polarization properties (Sec. VI), and the spectral features (Sec. VII).

### III. MEASUREMENT OF THE MATERIAL GAIN $g_{mat}$

In this Section, we report the measurement of the material gain  $g_{mat}$ , and then its estimation based on intrinsic characteristics of the gain medium.

#### A. Pump-probe experiment

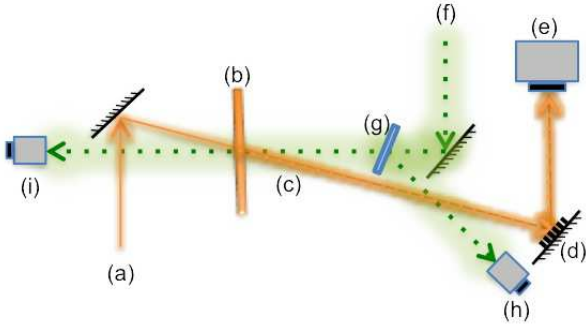


Figure 2: Pump-probe set-up for measuring the material gain  $g_{mat}$ . (a) Continuous probe beam. (b) Sample. (c) Amplified probe beam. (d) Monochromator. (e,h,i) Photodiodes. (f) Pulsed pump beam. (g) Glass slide.

We carried out pump-probe experiments to get the amplification factor, and then  $g_{mat}$ . The sample was a 18  $\mu\text{m}$  thick layer of PMMA [56], doped

with DCM (1.4 wt% with respect to PMMA [57]) and spin-casted on a glass slide. The set-up is described in Fig. 2. The pump beam is a frequency doubled Nd:YAG laser (532 nm, 10 Hz, 0.5 ns,  $\varnothing$  200  $\mu\text{m}$  [58]) and the probe beam is a Helium/Neon laser (594 nm, continuous,  $\varnothing$  65  $\mu\text{m}$ ). Both beams are incident on the sample at the Brewster angle to avoid parasitic reflections. They are not exactly parallel for experimental convenience, but their linear polarizations are parallel. The probe is collected on a rapid photodiode (rise time about 1 ns), which signal is sent to a 1 GHz oscilloscope triggered by the pump. A bump is visible, when the pump is on. A typical trace is presented in Fig. 3. Several tests were performed to ensure that the bump rightly comes from the probe amplification. In particular, a monochromator showed that there is no bump out of the probe wavelength (ie. 594 nm). Therefore the bump is not provided by fluorescence, but by stimulated emission.

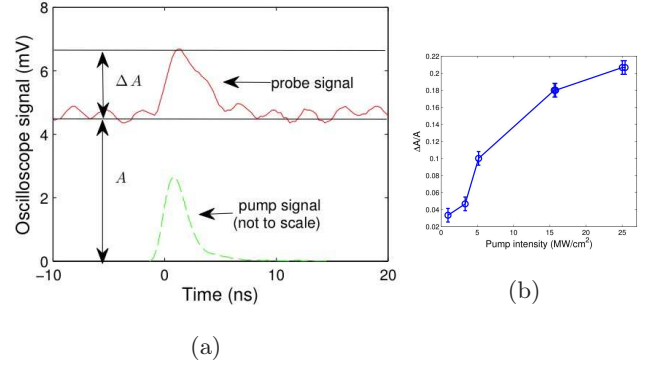


Figure 3: (a) Typical signals of the probe and pump beams detected by the photodiodes. (b) Amplification factor versus the pump intensity for a probe intensity  $I_{pr} = 435 \text{ W.cm}^2$ .

To infer the gain material  $g_{mat}$  and the gain efficiency  $K$  from the amplification factor  $\Delta A/A$  measured experimentally (Fig. 3), we wrote the equation of propagation of the probe intensity  $I_{pr}$ :

$$dI_{pr} = g_{mat} I_{pr} dz = K I_{pu} I_{pr} dz \quad (4)$$

which depends on the pump intensity  $I_{pu}$ . If the absorption of the pump is assumed to be negligible over the thickness  $h$  of the layer, then:

$$\frac{I_{pr}(h)}{I_{pr}(0)} = \frac{A + \Delta A}{A} = e^{K I_{pu} h} \quad (5)$$

As the amplification factor  $\Delta A/A$  is a small quantity (see Fig. 3), then it is proportional to the gain efficiency  $K$ :

$$\frac{\Delta A}{A} = K I_{pu} h \quad (6)$$

In practice, the absorption of the pump beam must be taken into account. Then, the factor  $h$  of Eq. (6) must be replaced by

$$h \rightarrow \frac{1 - e^{-\alpha h}}{\alpha}$$

where  $\alpha$  is the absorption coefficient of the material at the pump wavelength:  $\alpha = N_0\sigma_a(\lambda = 532\text{nm})$  [59]. As the temporal behavior of the amplification reproduces the temporal profile of the pump (see Sec. VIII), the variation  $\Delta A$  was measured at the maximum of the bump signal (see Fig. 3), and the factor  $I_{pu}$  involved in eq. (6) is the peak intensity of the pump at the entrance of the layer. The measured amplification factor  $\Delta A/A$  versus the peak intensity  $I_{pu}$  is plotted in Fig. 4 for different probe intensities. The whole set of experimental data is linearly fitted, the slope being proportional to the gain efficiency  $K$ , and leads to  $K = 20 \pm 5 \text{ cm.MW}^{-1}$ . Here the main source of uncertainty comes from the temporal profile of the pump beam (assumed to be gaussian) and its duration.

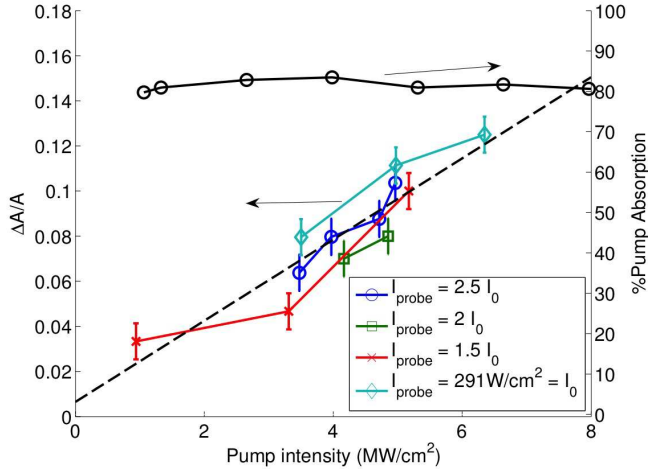


Figure 4: Amplification factor  $\Delta A/A$  (left axis) and absorption (right axis) versus pump intensity. The dotted line is a linear fit of the set of amplification factors measured at different probe intensities.

### B. Estimation of the gain efficiency

In addition, the gain efficiency  $K$  can be roughly estimated from the material characteristics, using the first term in Eq. (3):

$$g_{mat}^{594} = \sigma_e^{594} N^*$$

where  $N^*$  is the density of excited dye molecules. The vibrational states are known to relax in less than 1 ps [31, 32], so much faster than the timescale involved in this study. We assume then that the dye molecules can be considered as an effective two level system, where  $N_0$  is the density of dye molecules in the ground state and  $N = N_0 + N^*$  is the density of all the dye molecules. The triplet states are neglected, since the timescale involved in this study is much shorter than the typical time of the intersystem crossing (see Sec. VIII). The rate equation

for  $N^*$  follows then:

$$\frac{dN^*}{dt} = \sigma_a^{532} N_0 \frac{I_{pu}}{h\nu_{pu}} + \sigma_a^{594} N_0 \frac{I_{pr}}{h\nu_{pr}} - \sigma_e^{594} N^* \frac{I_{pr}}{h\nu_{pr}} - \frac{N^*}{\tau_f} \quad (7)$$

where  $\tau_f$  is the lifetime of fluorescence. In Sec. VIII, the time evolution of the stimulated emission is shown to reproduce the pump profile, which means that the gain medium responds instantaneously at the timescale of the pump variations. The gain medium can thus be considered in a stationary state. Hence the left part of Eq. (7) is zero, and  $N^*$  can be expressed as:

$$N^* = N \frac{\sigma_a^{532} \frac{I_{pu}}{h\nu_{pu}} + \sigma_a^{594} \frac{I_{pr}}{h\nu_{pr}}}{\sigma_a^{532} \frac{I_{pu}}{h\nu_{pu}} + \sigma_e^{594} \frac{I_{pr}}{h\nu_{pr}} + \frac{1}{\tau_f}} \quad (8)$$

The cross sections are evaluated in App. B. The second term in the numerator of  $N^*$  is several order of magnitude smaller than the first one, and is thus neglected. Similarly, as the  $I_{pr}/I_{pu} \sim 10^{-4}$ , the second term in the denominator is neglected, leading to:

$$N^* = N \frac{\sigma_a^{532} \frac{I_{pu}}{h\nu_{pu}}}{\sigma_a^{532} \frac{I_{pu}}{h\nu_{pu}} + \frac{1}{\tau_f}} \quad (9)$$

The linear regime presented in Fig. 4 correspond to the case:

$$\sigma_a^{532} \frac{I_{pu}}{h\nu_{pu}} \ll \frac{1}{\tau_f} \quad (10)$$

which means that  $I_{pu}$  should be less than  $8 \text{ MW.cm}^2$ , in agreement with Fig. .... In the linear regime, expression (9) leads to the following expression for the gain efficiency:

$$K = \sigma_e^{594} \frac{N^*}{I_{pu}} = \sigma_e^{594} \sigma_a^{532} N \frac{\tau_f}{h\nu_{pu}} \quad (11)$$

In Sec.VIII,  $\tau_f$  was measured and is about 2 ns. The other quantities involved in expression (11) are estimated in App. B, and leads to  $K \simeq 300 \text{ cm.MW}^{-1}$ , so more than 10 times higher than the experimental value. This discrepancy may originate from intermolecular processes, which reduce the number of excited molecules actually involved in stimulated emission. In particular, it must be stressed that the concentration of DCM in PMMA was hereafter set to 5 wt%, since it gives the maximal observed gain in ASE configuration (see Sec. IV B). A higher dye concentration leads to a strong quenching and then to a significant decrease of stimulated emission efficiency.

The conclusion of this Section on the gain material  $g_{mat}$  is that it can be measured by the means of a pump-probe set-up and leads to the gain efficiency  $K = 20 \text{ cm.MW}^{-1}$  at 594 nm for 1.4 wt% of DCM in PMMA pumped at 532 nm. However a theoretical derivation often gives an overestimation because of intermolecular processes, which are difficult to evaluate.



#### IV. MODAL GAIN $g_{mod}$

In this section, we evaluate the influence of the geometry on gain values, both theoretically in subsection IV A and experimentally in subsection IV B.

##### A. Confinement factor

In this subsection, we estimate the field confinement factor  $\Gamma$  on the example of the dye-doped organic thin films, which are experimentally investigated in subsection IV B.

The confinement factor  $\Gamma$  was introduced in Eq. (1) and accounts for the transverse overlap of the material gain  $g_{mat}$  with the pump  $E_p$  and lasing  $E_l$  mode profiles inside the layer. Then it depends on the specific lasing mode  $E_l$  which is considered. Eq. (1) is an approximation of a more general expression, which involves the spatial profiles of the fields and the gain efficiency:

$$g_{mod} = \frac{\int d\vec{r} K(\vec{r}) |E_p(\vec{r})|^2 |E_l(\vec{r})|^2}{\int d\vec{r} |E_l(\vec{r})|^2} - \alpha_{mod} \quad (12)$$

For the sake of simplicity, we assume that the field profiles are uniform within the sample plane (along x and y-axes), and consider only field variations along the layer width (z-axis). Then, in the case of an homogeneous distribution of dyes in the slab (ie.  $K$  is constant), the modal gain reduced to eq.(1) with a confinement factor  $\Gamma$  given by [? ? ]:

$$\Gamma = \frac{\int d\vec{r} |E_p(\vec{r})|^2 |E_l(\vec{r})|^2}{\int d\vec{r} |E_p(\vec{r})|^2 \int d\vec{r} |E_l(\vec{r})|^2} \quad (13)$$

with  $\int d\vec{r} |E_p(\vec{r})|^2 = I_{pu}$ .

The field distribution at the pumping wavelength corresponds to the absorption distribution. Then it describes the profile of excited molecules in the layer. The confinement factor in its turn describes the overlap between the gain region and the emission field, and can be estimated numerically through the calculation of the electric field distribution in the film at pump and emission wavelength. It is absolutely essential to account for the material absorption spectrum, as absorption coefficient actually defines the pump field distribution in the thin film.

For the pump field, we consider a standing wave problem in the two-layered system: the dye doped polymer with  $n_1 = 1.54$  and variable thickness  $h_1$  and the  $\text{SiO}_2$  layer ( $n_2 = 1.46$ ,  $h_2 = 2\mu\text{m}$ ) placed between the semi-infinite medium (air,  $n_0 = 1$ ) and the substrate (Si,  $n_3 = 4.14$ ). For the propagating laser field, we use the model of the effective index described in [33], and consider the first vertical excitation with TE polarization, which means that the electric field lies in the plane of the layer.

The confinement factor was then numerically estimated based on Eq. (13) at several emission wavelengths around

600 nm (Fig. 5a). The variation of absorption between simulated dye-doped layers influences first of all the absolute value of the confinement factor. It may appear from the first glance that strongly absorbing media has lower confinement factor. Yet, this is a matter of a mismatch between the pumping and emission fields, especially relevant in the vicinity of the air-polymer surface for strongly absorbing media.

In fact, Fig. 5a represents the confinement factor of the material with a homogeneous spectral distribution of the emission. In the emission cross section ( $\bar{\sigma}_e(\lambda_f)$ , Fig. 5b) contributes to the emission efficiency and thus must be taken into account to estimate the value and spectral position of the actual confinement factor (Fig. 5c):

$$\Gamma^*(\lambda_f) = \bar{\sigma}_e(\lambda_f) \Gamma(\lambda_f) \quad (14)$$

The highest peak in such graph provides information about the confinement factor and the center of the emission spectrum. For instance, a 600nm-thick PM605-doped PMMA layer emits around 580 nm, while DCM and RH640-doped layers tend to emit at longer wavelengths (about 620 nm).

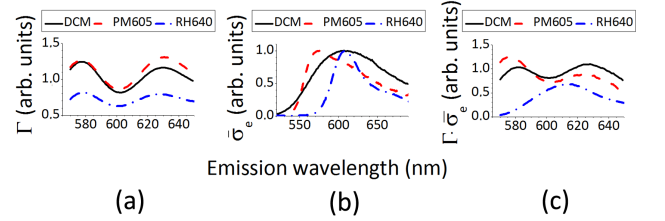


Figure 5: Estimation of the confinement factor in a 600 nm 5wt% dye-doped PMMA layer for DCM, RH640 and PM605 dyes: (a)  $\Gamma$  estimated based on Eq. (13); (b) normalized emission cross-sections; (c) actual  $\Gamma$  accounting for the spectral distribution of the stimulated emission.

Finally, we examine the influence of the thickness of the dye-doped PMMA layer on the confinement factor  $\Gamma$ . The results are gathered in Fig. 6. In general, the increase of the layer thickness results in a decrease of  $\Gamma$ , and thus of the gain. Actually the absorption of the pump leads to a non-homogeneous excitation profile within the layer. Thereby, the increase of the layer thickness does not provide the better overlap of the excitation and emission patterns. The emission wavelength is also impacted by the layer thickness, as shown in Fig. 6b.

In conclusion, the amplification properties are strongly influenced by the exact geometry of the system, as well as by the absorption and emission features of gain material. The confinement factor is an appropriate tool to take into account such parameters.

##### B. VSL method

To evaluate the influence of the device geometry, we measure the modal gain  $g_{mod}$  with the Variable Stripe

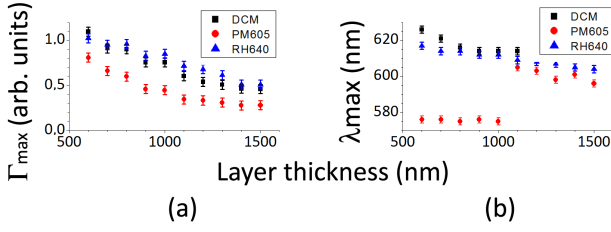


Figure 6: Confinement factor (a) and the center of the emission spectrum (b) as a function of thickness of the dye-doped polymer layer.

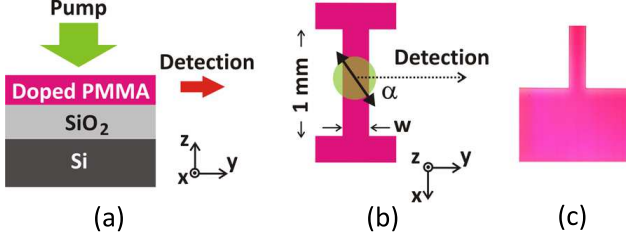


Figure 7: Experimental configuration: (a) The sample stack. (b) In-plane scheme of a ribbon resonator. (c) Optical micro-scope photo in real colors of a 165  $\mu\text{m}$  PMMA-PM605 ribbon micro-laser (partial view).

Length (VSL) technique [27] for the stack layer used in Section V. The sample geometry is described in Fig. 7a. The 600 nm thick PMMA layer was doped with 5 wt% DCM and spin-coated on a commercial 2  $\mu\text{m}$  SiO<sub>2</sub>/Si wafer. It then sustains a single vertical ( $z$  axis) excitation for each polarization of the propagating field [33].

The experiment was described in [34]. The sample is pumped from the top (along the  $z$  axis) by a frequency doubled Nd:YAG laser (532 nm, 500 ps, 10 Hz), which beam was shaped as a rectangle of fixed width (about 300  $\mu\text{m}$ ) and variable length  $L$ . Then the emitted intensity is collected at the sample edge, in the layer plane ( $xy$  plane), and the modal gain can be inferred from its variation with the length  $L$  at a fixed pump intensity. As shown in Fig. 8, the modal gain varies linearly with the pump intensity, reinforcing Eq. 2. The gain efficiency was then inferred from a linear fit:  $K = 41 \pm 2 \text{ cm.MW}^{-1}$ .

## V. THRESHOLD ESTIMATE

The gain efficiency  $K$  can be used to quantitatively predict the lasing threshold intensity, which is evidenced in this section on the example of Fabry-Perot micro-lasers.

The device is described in Fig. 7. The cavity is fabricated by electron-beam lithography - which ensures a nanoscale etching quality [35] - within the stack which was investigated in subsection IV B. The gain efficiency

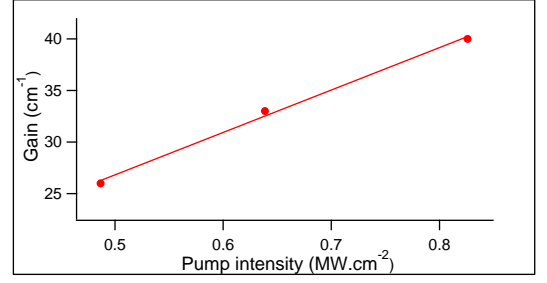


Figure 8: Modal gain versus pump intensity for a 600 nm thick 5 wt% DCM-doped PMMA layer on a 2  $\mu\text{m}$  SiO<sub>2</sub>/Si layer, measured by VSL method.

$K$  measured by VSL should then be still valid. To obtain a Fabry-Perot resonator, a ribbon shape was chosen. Ribbon cavities were fabricated with different widths  $w$  ranging from 100  $\mu\text{m}$  to 200  $\mu\text{m}$ . As shown in Fig. 7b, there is no border in the  $x$ -direction, in order to prevent back reflection along the  $x$ -axis, and therefore avoid mode competition, which would modify lasing thresholds. We then expect Fabry-Perot modes propagating along the  $y$ -axis. The emission is collected sideways in the layer plane along the  $y$ -direction and analyzed by an Acton-research 2500i spectrometer coupled to a cooled CCD camera. Typical Fabry-Perot spectra are presented in Fig. 1.

The pump laser was similar as that used for VSL experiments (532 nm, 500 ps, 10 Hz) and the setup provides an uniform pumping (within the ribbon width) from the top (along  $z$ -axis). The energy and linear polarization of the pump beam are controlled independently with a standard combination of linear polarizers and half-wave plates. The polarization of the pump beam lies in the  $xy$ -plane and its orientation in this plane is defined by the angle  $\alpha$  with respect to the  $y$ -axis (see Fig. 7b), namely  $\alpha = 0^\circ$  if the polarization is oriented along the  $y$ -axis, and  $\alpha = 90^\circ$  if the pump polarization is along the  $x$ -axis. The influence of  $\alpha$  is discussed in Section VI. Here, we consider only the case  $\alpha = 90^\circ$  which was used in VSL experiments. Fig. 9b shows a typical curve, where the threshold intensity  $I_{th}$  is clearly identified as a change of slope with a precision of about 0.1 MW.cm<sup>-2</sup>.

To predict the threshold intensity, we assume that the stationary regime was reached. This issue will be discussed in Section VIII. In that case, the threshold is determined by the gain (and thus the pump intensity  $g_{th} = KI_{th} - \alpha_{mod}$ ) necessary to compensate the losses:

$$re^{g_{th}2w} = 1 \quad (15)$$

with  $r$  standing for the total losses in the system. For the sake of simplicity, we only consider refraction losses:  $r = R^2$ , where  $R = \left(\frac{n-1}{n+1}\right)^2 \simeq 0.04$  is the reflection coefficient at the boundary ( $n \simeq 1.5$ ). Pump intensity at the threshold is then expected to be linear with  $1/w$ ,

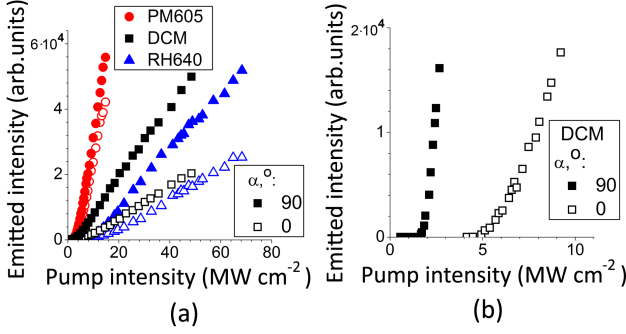


Figure 9: Influence of the pump polarization  $\alpha$  on the emission versus pump intensity in the case of a) ASE, b) a 165  $\mu\text{m}$  DCM ribbon micro-laser.

leading to the following relation:

$$I_{th} = -\frac{\ln R}{K} \frac{1}{w} + \frac{\alpha_{mod}}{K} \quad (16)$$

Threshold measurements were carried out for three dyes as reported in Fig.10 and pumping intensities at threshold show indeed a linear behavior with  $1/w$ . Moreover, a quantitative agreement with Eq.(16) is demonstrated for DCM, using  $R = 0.04$  and  $K = 41 \text{ cm.MW}^{-1}$ , without adjusted parameter (see Fig.10a).

This agreement implies several consequences. Firstly the assumption of a stationary regime should be valid. Secondly spatial hole-burning does not influence the thresholds, whereas dye molecules lead to an homogeneous gain and the spectra are multimode, even at threshold (see Fig. 1). Thirdly only the losses due to refraction are taken into account in Eq. (16). Hence the quantitative agreement means that the losses due to diffraction at the cavity edges do not modify the thresholds, as evidenced in [37], and that the Fresnel coefficient for an infinite wall  $R$  does reproduce correctly the refraction at the boundary, even if the cavity thickness scales with the wavelength.

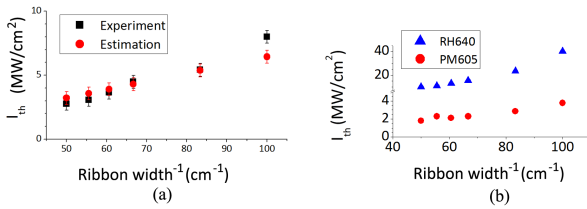


Figure 10: Experimental threshold intensities versus  $1/w$  [see Eq. (16)] at  $\alpha = 90^\circ$  with different laser dyes: (a) DCM (together with estimated values), (b) PM605 and RH640.

Fig.10 also shows a deviation from linear behavior for the smallest cavities. More intricate active phenomena occur in these cases and will be discussed in Sec.VII. Reciprocally, Eq. (16) can be used to infer the gain efficiency of each dye-doped PMMA layer. The fit results are given in Table I.

Table I: Comparison of gain efficiencies  $K$  for different dye-doped PMMA layers inferred by fitting data of Fig.10 with Eq. (16), using  $r = R^2 = 0.04^2$ .

Dye	DCM	RH640	PM605
$K [\text{cm MW}^{-1}]$	$42 \pm 4$	$9 \pm 1$	$81 \pm 2$

To summarize, we evidenced that gain efficiency  $K$  inferred by VSL technique in Section IV B is consistent with threshold measurements. Moreover, predictions can be made with good precision (less than 10 % of uncertainty). By the way, Eq. (16) can be used to estimate unknown resonance losses, as it was demonstrated for square-shaped micro-lasers in [these-Iryna] Section 6.1.5.

## VI. IMPACT OF THE PUMP POLARIZATION

This section focuses on the influence of the pump polarization on gain. Actually, ASE intensity and laser threshold depend on the pump polarization, up to a factor of three. The nature of the effect is explained and a model is provided, giving a quantitative agreement for the three laser dyes.

Amplification in organic materials is in general anisotropic, as reported in [22], and the pump polarization plays a role in the orientation of the main axis of amplification. In fact, dye molecules can be considered as fixed and non-interacting dipoles in the time scales involved in this study (see Section VIII). Each molecule absorbs preferentially along the direction of its absorption dipole, and emits a fluorescent photon according to its emission dipole. Both dipoles depend on the geometry of the molecular structure. This explains, that an ensemble of dye molecules can emit fluorescence in specific directions (monitored by the pump polarization), even if they are isotropically distributed. This phenomenon is known as fluorescence anisotropy and has generated a broad literature (see [31] and [32] for a review). This effect was used for instance in Organic Light Emitting Diodes, aligning the molecules to optimize the emission [1]. Here, we focus on the consequences on stimulated emission and gain. Theories were developed to account for amplification anisotropy [38–41], however we will show hereafter, that it can be described in the framework of fluorescence anisotropy, in good agreement with experiments.

We experimentally investigated the influence of the pump beam polarization on ASE and lasing thresholds, using samples and experimental set-up described in Sections IV and V. The direction of observation remains along the width of the ribbon (y-axis in Fig.7b), while the linear pump beam polarization lies in the substrate plane and is varied between perpendicular ( $\alpha = 90^\circ$ ) and parallel ( $\alpha = 0^\circ$ ) to the y-axis. Fig.9 presents the emitted intensity versus the pump intensity in ASE and Fabry-Perot configurations. It suggests, that the pump

polarization  $\alpha$  is a relevant parameter, which influence is strongly related to the molecular structure of the dye. For instance, the laser threshold is reduced by a factor of three from  $\alpha = 0^\circ$  to  $90^\circ$  for DCM (Fig.9b), which can be considered as a linear dipole due to its linear molecular structure, while the ASE curves remain almost unmodified for PM605 (Fig.9a), which molecular skeleton looks more rounded.

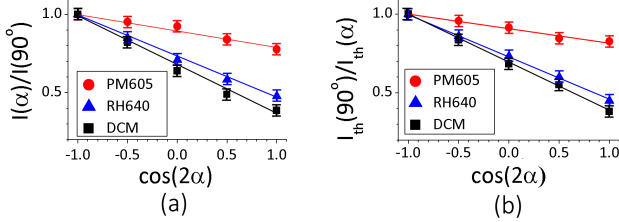


Figure 11: Role of the pump beam polarization on stimulated emission. (a) ASE in dye-doped PMMA thin film. (b) 180  $\mu\text{m}$  Fabry-Perot micro-lasers. The pump beam polarization  $\alpha$  is defined on Fig.7.

To predict the dependance on  $\alpha$ , we use a model based on fluorescence anisotropy [32, 42, 43], which accounts for a given distribution  $f$  of fixed and non-interacting dyes. The emitted intensity  $I_e$  is proportional to an integral over all the possible orientations  $\Omega$  of a molecule:

$$I_e(\alpha) \propto \int_{\Omega} P_{abs}(\alpha, \Omega) P_{em,y}(\Omega) f(\Omega) d\Omega \quad (17)$$

Here  $P_{abs}$  stands for the probability of pump absorption and is then proportional to a cosinus squared between the pump and the absorption transition dipole of the molecule. Respectively  $P_{em,y}$  stands for the emission probability in the  $y$  direction and is then a sinus squared between the  $y$  direction and the transition emission dipole of the molecule. Hence we must introduce the angle  $\beta$  between the absorption and emission momentum of the dipole, which is known to be a constant, depending only on the molecular structure of the dye [44].

To calculated expression (17), we must choose an appropriate distribution  $f$ . For instance,  $f$  is constant for an isotropic distribution of molecules. In practice and as evidenced by ellipsometry measurements, spin-coating slightly aligns the molecules in the layer plane. So we introduce an angle  $\theta_0$ , such that  $f$  is constant between  $-\theta_0$  and  $+\theta_0$  and zero outside (see Fig.17). A more comprehensive study is reported elsewhere [42]. Here we skip the details and go directly to the formula [60]:

$$\frac{I_e(\alpha)}{I_e(\alpha = 90^\circ)} = \frac{\rho + 1}{2} + \frac{\rho - 1}{2} \cos 2\alpha, \quad (18)$$

where  $\rho = \frac{I_e(0^\circ)}{I_e(90^\circ)}$  is a positive function of  $\theta_0$  and  $\cos^2 \beta$ , and is described in Appendix A. As expected, the emitted intensity  $I_e$  is maximal for  $\alpha = 90^\circ$ , which was the configuration considered for VSL and threshold measurements

Table II: Comparison of  $\rho$  values obtained from ASE and laser threshold

$\rho$	DCM	PM605	RH640
ASE	$0.33 \pm 0.03$	$0.77 \pm 0.03$	$0.46 \pm 0.03$
Threshold	$0.38 \pm 0.03$	$0.84 \pm 0.03$	$0.48 \pm 0.04$

( Sections IV B and V). For a linear dipole ( $\beta = 0$ ) and an isotropic 3D distribution ( $\theta_0 = 90^\circ$ ), then  $\rho = 1/2$ , which means, that half of the light is emitted in the  $y$ -direction, even if the pump polarization is parallel to the  $y$ -direction.

$I_e(\alpha)$  describes the probability of fluorescence emission. Hence it is likely that the ASE intensity is proportional to  $I_e$ . First we checked that the ratio  $\frac{I_e(\alpha)}{I_e(90^\circ)}$  does not significantly depend on the pump intensity, namely the fluctuations remain in the range of  $\pm 1\%$  for pump intensity varying from 4 to 80  $\text{MW.cm}^{-2}$ . Then the average ratio  $\frac{I_e(\alpha)}{I_e(90^\circ)}$  is plotted versus  $\cos(2\alpha)$  in Fig.11a for the three dyes. The curves present a linear behavior, evidencing the validity of formula (18), even in the stimulated regime. The  $\rho$  values presented in Table II are then inferred from the linear fits and formula (18).

Validity of exp. (18) can be checked for lasing thresholds as well. In fact they can be considered as working points where the non-linear behavior is still relatively low and fluorescence formula like Eq.(17) should then apply [43, 45]. The gain value  $g_{th}$  necessary to attain the lasing threshold is determined by losses, which does not depend on  $\alpha$ , leading to  $K(\alpha)I_{th}(\alpha) = g_{th} = \text{const.}$  Thereby, we expect the ratio of threshold intensities  $I_{th}(\alpha)/I_{th}(90^\circ)$  of the ribbon-shaped micro-lasers to be inversely proportional to  $K(\alpha)/K(90^\circ)$ . This ratio is then plotted versus  $\cos(2\alpha)$  in Fig.11b for  $w=180 \mu\text{m}$  Fabry-Perot micro-lasers and shows indeed a linear behavior for the three dyes. If the ratio  $I_{th}(90^\circ)/I_{th}(\alpha)$  is assumed to be equal to the right part of Eq. (18), then a  $\rho$  value can be inferred for each of the dyes. The results are gathered in Tab.II where the error bars correspond to the fluctuations for ribbon widths varying from 150 to 200  $\mu\text{m}$ .

Experimental results, presented in this section, were obtained under linear pumping beam polarization. In fact, emission under circularly-polarized excitation can be described in the same terms based on eq(18). Indeed, integration over  $\alpha$  provides  $\frac{I(\text{circular})}{I(\alpha=90^\circ)} = \frac{\rho+1}{2} < 1$ , meaning that pumping with circular polarization is less efficient compared to linear polarization with  $\alpha = 90^\circ$ . This ratio was verified for a 165  $\mu\text{m}$  DCM ribbon micro-laser and gave a  $\rho$  value identical to Tab.II.

For completeness, the  $\rho$  values should be inferred as well in the fluorescence regime. However the high doping rate of the layers favors energy transfer from dye to dye and tends to make the emission isotropic [46]. Such an isotropization ( $\rho = 1$ ) does not occur obviously in our stimulated systems (ASE and laser), because energy



transfer is prevented due to its characteristic time typical of spontaneous processes, and then much longer than stimulated emission. The different time scales are evidenced in Sec. VIII.

To summarize, the  $\rho$  parameter quantifies the sensitivity to polarization. It is specific of a dye molecule and its distribution in the layer. Such agreement between the  $\rho$  values inferred from both ASE and lasing experiments for the three dyes stresses the validity of our assumptions as well as the interest of such an approach for predictions of gain properties.

## VII. SPECTRAL FEATURES

Laser spectra from organic-based devices are in general multimode and inscribed in an envelope (Fig.1). The distribution of the lasing peaks is mostly determined by the resonator shape and is discussed elsewhere [47]. Here, we focus on the envelope, which depends on the gain medium, in particular its width and central wavelength, which are relevant for designing of electrically-pumped organic lasers.

### A. Width of the spectral envelope

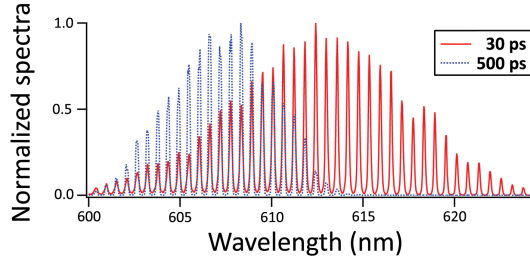


Figure 12: Influence of the pump beam duration (30 ps or 500 ps) on the spectral envelope of a square-shaped micro-laser. The gain material is PMMA doped with 5 wt% of DCM.

In this subsection, we consider the width of the spectral envelope. First, it must be stressed that it strongly depends on the pump duration. For instance, in Fig. 12, we superimposed two spectra of the same micro-laser in identical experimental conditions. The set-up and the 500 ps pump laser were described in Section V. The 30 ps pump laser is a frequency doubled Nd:YAG laser (532 nm, 10 Hz). As evidenced in Fig. 12, the peaks does not move, but the Full Width at Half Maximum (FWHM) of the envelope is about twice larger for the 30 ps pump pulse compared to the usual 500 ps pump pulse. This can be accounted for by the laser dynamics [48] and the balance between the duration of the pump and the photon lifetime ( $\sim 1$  ps for a  $w=200$   $\mu\text{m}$  Fabry-Perot cavity). For the usual 500 ps pump laser, FWHM of ASE is about

10-20 nm depending on the dye, while FWHM of fluorescence is of the order of 50-100 nm. The FWHM of the lasing spectra depends on the resonator shape. For instance, we noticed that the FWHM of Fabry-Perot spectra is typically four times narrower than the FWHM of ASE. In general, spectra associated with whispering gallery modes are broader.

### B. Maximum of the spectral envelope

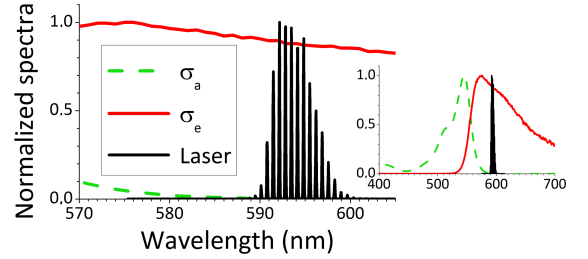


Figure 13: Absorption and emission properties of 5 wt% of PM605 in PMMA. Normalized absorption ( $\sigma_a$ ) and stimulated emission ( $\sigma_e$ ) cross sections, and normalized emission spectrum of a 150  $\mu\text{m}$  ribbon micro-laser.

Fig. 13 evidences that the envelope of the lasing spectrum is not centered at the maximum of the fluorescence spectrum. Here, following Mazumder et al. [49], we propose a simple explanation based on re-absorption. Due to the overlap between absorption ( $\sigma_a(\lambda)$ ) and stimulated emission ( $\sigma_e(\lambda)$ ) cross sections, unexcited molecules can absorb photons emitted from excited states, which decreases the gain:

$$g(\lambda) = \sigma_e(\lambda) N^* - \sigma_a(\lambda) (N - N^*) \quad (19)$$

where  $N$  stands for the total density of dye molecules and  $N^*$  for the density of excited dye molecules. Hence, the ratio of molecules  $\gamma(\lambda) = N_{th}^*/N$  that must be excited to reach the threshold depends on re-absorption [29, 49]:

$$\gamma(\lambda) = \frac{N^*}{N} = \frac{g(\lambda) + \sigma_e N}{\sigma_a(\lambda) N} \quad (20)$$

At threshold, the gain balances the losses, and  $g(\lambda)$  can be substituted by  $-\ln R/w$  for a Fabry-Perot resonator (see Eq. 15).  $\gamma(\lambda)$  was plotted in Fig.14b for different widths  $w$  of the Fabry-Perot ( $\ln R$  remains unchanged) using  $\sigma_e$  and  $\sigma_a$  determined in Appendix B. Each curve shows a minimum, which corresponds to the lasing wavelength close to threshold. The minimum of  $\gamma$  is blue-shifted when the width of the Fabry-Perot decreases, i.e. when the loss of the cavity increases. The order of magnitude is consistent with the experimental observations summarized in Fig.14a. A similar effect was reported using absorbers in micro-droplets [49, 50].

In other words, the envelope of the lasing spectrum is blue-shifted, when the quality factor of the resonator decreases [23]. Measurements of such spectral shifts for a given gain material would provide a solid basis for the experimental estimation of the cavity properties through the spectroscopic study of the laser effect. Anyway, as the shift can be larger than a dozen of nanometers, it must be taken into account to optimize the architecture of the device in the context of electrically pumped organic lasers.

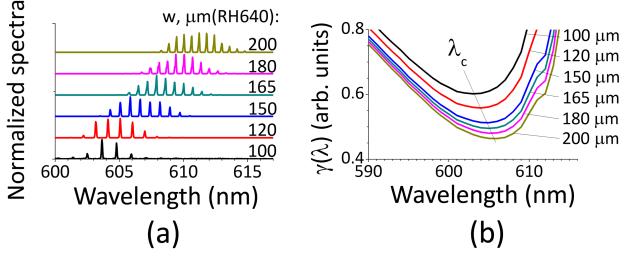


Figure 14: Influence of losses on the spectral envelope: (a) experimental spectra of Fabry-Perot cavities of different widths  $w$  under the same pump intensity; (b) calculated threshold condition  $\gamma(\lambda)$  (Eq.20) for Fabry-Perot cavities of different widths. The gain material is PMMA doped with 5 wt% of RH640.

### VIII. TEMPORAL BEHAVIOR

This last Section focuses on experimental studies of the temporal properties of spontaneous and stimulated emission in dye-doped polymer thin films. The dye-doped PMMA layers described in Section IV B were pumped with a frequency doubled Nd:YAG laser (10 Hz, 532 nm, 35 ps) and the emission was collected through a monochromator and then injected into a streak camera (Optoscope by ARP) with about 8 ps temporal resolution. Fig. 15 presents a simplified scheme of the setup. In order to prevent the influence of guiding effects, the layers used for fluorescence study were directly spin-coated on a Si substrate and  $\theta = 55^\circ$ , while a SiO<sub>2</sub>/Si substrate was used for ASE and Fabry-Perot samples with  $\theta = 0^\circ$ .

As evidenced in Fig.16, the temporal behavior of the ASE signal replicates that of the pump (except for RH640, which exhibit a small exponential relaxation of ASE, not shown here), whereas the fluorescence emission occurs over a longer time scale. Measured fluorescence lifetimes were 1.8 ns for DCM, 2.6 ns for RH640 and 1.5 ns for PM605, in consistence with results measured elsewhere [51]. Regarding the lasing emission from a Fabry-Perot cavity, Fig. 16b evidences that it is delayed of about 20 ps. This delay decreases if the pump intensity increases and the Fabry-Perot width  $w$  decreases, as expected since the build-up time of the laser emission

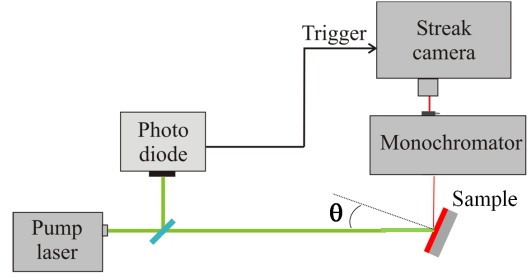


Figure 15: Scheme of the setup used for temporal studies. The retardation line is not shown. For ASE and Fabry-Perot measurements,  $\theta$  is set to zero, and the emission is collected in the plane of the layer. For fluorescence measurements,  $\theta = 55^\circ$  in order to prevent propagation effects.

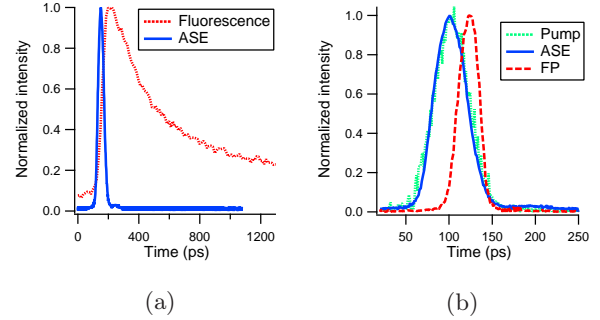


Figure 16: Dynamics of the spontaneous and stimulated emissions in a layer of PMMA polymer doped with 5 wt% of DCM: (a) fluorescence and ASE, (b) Pump signal, ASE, and lasing emission from a Fabry-Perot cavity of width  $w = 200 \mu\text{m}$  just above the threshold. Averaging over 20-100 pump pulses.

decreases as well. It can be noticed that no spiking is observed, contrary to [24], maybe due to the shorter pump pulse.

### IX. CONCLUSION

In this paper, we have investigated the amplification properties of dye-doped polymer thin films. The gain efficiency  $K$  was introduced to facilitate the comparison between different materials in various configurations. It represents the linear ratio between gain and pump intensity, in the limit of validity of such linear behavior. It allows to derive a simple relation between gain, losses and threshold, which was experimentally validated in the benchmarking case of Fabry-Perot planar micro-lasers, demonstrating the reliability of this approach to select gain material in the framework of electrically pumped hybrid organic-inorganic devices.

The bulk gain was measured with a pump-probe setup and led to  $K = 20 \text{ cm.MW}^{-1}$  at 594 nm for 1.4 wt% DCM doped in PMMA pumped at 532 nm. The theoretical prediction overestimates its value by more than one order of magnitude, probably because of intermolecular

processes which are strongly involved in such materials. Several parameters alter the bulk gain and must be taken into account to design an actual device. First, the confinement factor  $\Gamma$  includes the geometrical features and the overlap between the pump beam and the propagating laser field. It varies typically from 0.5 to 2. Then, the intrinsic anisotropy of the molecular structure induces a sensitivity to the polarization of the pump beam, and can modify the gain up to a factor of three. By the way, we showed that the gain measurement is sensitive to the anisotropic distribution of the dye molecules within the layer, and provides therefore an indirect method to estimate it. Finally, the width of the gain spectrum, as well as its central wavelength, are monitored by reabsorption processes, and can be relatively well predicted. For all these parameters, we provided appropriated experiments in good agreement with theoretical predictions and consistent with the measured value of the bulk gain.

Besides, time resolved measurements were carried out at the picosecond scale. They showed that ASE reproduces the profile of the pump beam, which implies that the amplifying medium can be considered in a stationary regime with respect to the variations of the pump. Moreover, the build-up time of the laser emission was evidenced on the example of Fabry-Perot cavities of various widths.

In conclusion, we proposed a protocol for the analysis of gain properties of organic materials, and demonstrated that several parameters must be taken into account to reliably predict the laser threshold of the device. We hope that this work helps to pave the way towards an electrically pumped hybrid organic-inorganic laser.

### Acknowledgments

The authors acknowledge J. Delaire, F. Bretenaker, C. Lafargue and J. Lautru for stimulating and fruitful discussions.

### Appendix A: Fluorescence anisotropy

Figure 17: Description of the system for the calculation of the emitted light

The  $\rho$  quantity mentioned in Sec.V, could be calculated from the  $r_0$  parameter, familiar in the field of fluorescence anisotropy. But in practice  $\rho$  depends also on the distribution of the dyes through  $\theta_0$  (see fig. 17), and then on the layer fabrication. Here we provide the exact expression of  $\rho$  following a mathematical derivation, which is described elsewhere [42]:

$$\rho = \frac{I_e(\alpha = 0)}{I_e(\alpha = 90)} = \frac{A_1(\beta) B_1(\theta_0) + A_2(\beta) B_2(\theta_0)}{A_1(\beta) B_1(\theta_0) + A_2(\beta) B_3(\theta_0)}$$

Here the functions  $A_i(\beta)$ , and  $B_i(\theta_0)$ :

$$\begin{aligned} A_1(\beta) &= 2 - 2 \cos^2 \beta, \\ A_2(\beta) &= 1 - 3 \cos^2 \beta, \end{aligned}$$

$$\begin{aligned} B_1(\theta_0) &= 30 + 10 \sin^2 \theta_0, \\ B_2(\theta_0) &= -15 - 10 \sin^2 \theta_0 + 9 \sin^4 \theta_0, \\ B_3(\theta_0) &= -45 + 10 \sin^2 \theta_0 + 3 \sin^4 \theta_0. \end{aligned}$$

have been introduced in the sake of compactness of Eq. (ro). In limit cases of 2-D and 3-D distributions it reduces to:

$$\rho_{2D}(\beta) = \frac{3 - \cos^2 \beta}{1 + 5 \cos^2 \beta}$$

$$\rho_{3D}(\beta) = 2 \frac{2 - \cos^2 \beta}{3 + \cos^2 \beta}$$

For instance, in the case of 2-D distribution (which most likely applies to spin-coated light-emitting polymers)... The higher  $\rho$  values obtained for PM650 and RH640 evidence a tendency to isotropize the emission, which can be explained by their relatively rounded molecular structure.

This  $\rho$  quantity could be calculated from the  $r_0$  parameter, familiar in the fields of fluorescence anisotropy. But in practice  $\rho$  depends on the distribution of the dyes (through  $\theta_0$ ) and then on the layer fabrication. For instance, in the case of 2-D distribution (which most likely applies to spin-coated light-emitting polymers [52])  $\rho = 1/3$  at  $\beta = 0$ , suggesting that in examined DCM-doped PMMA layer emission dipoles are mainly oriented within the layer plane (for  $\beta = 25^\circ$ , reported for DCM under excitation at 461 nm [46],  $\rho = 0.43$ ).

### Appendix B: Absorption and stimulated emission cross-sections

The factor  $\sigma_a(532)N$  is inferred from the absorption of the pump, see Fig. 4:

$$e^{-\sigma_a(532)Nh} \simeq 0.2 \rightarrow \sigma_a(532)N \simeq 9.10^2 \text{cm}^{-1}$$

The emission cross-section is shaped as the fluorescence spectrum  $f(\lambda)$ :

$$\sigma_e(\lambda) = \frac{\phi \lambda^4}{8\pi n^2 c \tau_f} \frac{f(\lambda)}{\int f(\lambda) d\lambda} \quad (\text{B1})$$

Moreover the absorption and emission cross-sections are connected via:

$$\frac{\sigma_a^{max}}{\sigma_e^{max}} = \frac{1}{\phi} \frac{\lambda_e}{\lambda_a} \quad (\text{B2})$$

which stresses that the emission cross section is always smaller than the absorption cross section.

- 
- [1] S. Miyata and H. Sasabe, *Poled Polymers and Their Application to SHG and EO Devices*, CRC Press; 1 edition, 1997.
- [2] S. Miyata and H. S. Nalwa, *Organic Electroluminescent Materials and Devices*, CRC Press; 1 edition, 1997.
- [3] J. Shinar, *Organic Light-Emitting Devices: A Survey*, Springer; 2004.
- [4] Y. Koike, Japanese Journal of Applied Physics, **47**, 6629 (2008).
- [5] Organic nonlinear optics, J. Mater. Chem., themed issue, **19**, 7381 (2009).
- [6] C. Y. Chao and L. J. Guo, IEEE J. Sel. Top. Quant. Electron., **12**, 148 (2006).
- [7] I. D. W. Samuel, E. B. Namdas, G. A. Turnbull, Nature Photonics **3**, 546 (2009).
- [8] M. A. Baldo, R. J. Holmes, S. R. Forrest, Phys. Rev. B **66**, 035321 (2002).
- [9] I. D. W. Samuel, G. A. Turnbull, Chem. Rev. **107**, 1272 (2007).
- [10] S. Chénais, S. Forget, Polym. Int. **61**, 390 (2012).
- [11] M. Segal, M. A. Baldo, R. J. Holmes, S. R. Forrest, Z. G. Soos, Phys. Rev. B, **68**, 075211 (2003).
- [12] M. A. Baldo, R. J. Holmes, S. R. Forrest, Phys. Rev. B, **66**, 035321 (2002).
- [13] N.C. Giebink, S.R. Forrest, Phys. Rev. B, **79**, 073302 (2009).
- [14] N. Tessler, D. J. Pinner, V. Cleave, D. S. Thomas, G. Yahioğlu, P. Le Barny, and R. H. Friend, Appl. Phys. Lett., **74**, 2764 (1999).
- [15] V.G. Kozlov, G. Parthasarathy, P.E. Burrows, V.B. Khalfin, J.Wang, S.Y. Chou, S.R. Forrest, IEEE Journal of Quantum Electronics, **36**, 18 (2000).
- [16] M.D. McGehee, A.J. Heeger, Adv. Mater. **12**, 1655 (2000).
- [17] R. Gupta, M. Stevenson, A. J. Heeger, J. Appl. Phys., **92**, 4874 (2002).
- [18] Voss T., Scheel D., Schade W., “A microchip-laser-pumped DFB-polymer-dye laser” App. Phys. B: Lasers and Optics, **73**, 105 (2001).
- [19] Riedl T., Rabe T., Johannes H.-H., Kowalsky W., Wang J., Weimann T., Hinze P., Nehls B., Farrell T., Scherf U., Appl. Phys. Lett., **88**, 241116 (2006).
- [20] A. E. Vasdekis, G. Tsiminis, J.-C. Ribierre, L. O’ Faolain, T. F. Krauss, G. A. Turnbull, I. D. W. Samuel, Opt. Express, **14**, 9211 (2006).
- [21] Y. Yang, G. A. Turnbull, I. D. W. Samuel, Appl. Phys. Lett., **92**, 163306 (2008).
- [22] I. Gozhyk, G. Clavier, R. Méallet-Renault, M. Dvorko, R. Pansu, J.-F. Audibert, A. Brosseau, C. Lafargue, V. Tsvirkun, S. Lozenko, S. Forget, S. Chénais, C. Ulysse, J. Zyss, and M. Lebalental, Phys. Rev. A **86**, 043817 (2012).
- [23] S. Y. Lam and M. J. Damzen, Appl. Phys. B, **77**, 577 (2003).
- [24] V. Bulovic, V. G. Kozlov, V. B. Khalfin, S. R. Forrest, Science, **279**, 553 (1998).
- [25] W. Lu, B. Zhong, D. Ma, Appl. Opt. **43**, 5074 (2004).
- [26] A. Costela, O. Garcia, L. Cerdan, I. Garcia-Moreno, R. Sastre, Opt. Express **16**, 7023 (2008).
- [27] L. Dal Negro, P. Bettotti, M. Cazzanelli, D. Pacifici, L. Pavesi, Opt. Commun., **229**, 337 (2004).
- [28] L.A. Coldren, S.W. Corzine, *Diode Lasers and Photonic Integrated Circuits*, Wiley Series in microwave and optical engineering: 1995.
- [29] O. G. Peterson, J. P. Webb, W. C. McColgin, J. H. Eberly, J. Appl. Phys. **42**, 1917 (1971).
- [30] A. Tagaya, Y. Koike, E. Nihei, S. Teramoto, K. Fujil, T. Yamamoto, K. Sasaki, Appl. Opt. **34**, 988 (1995).
- [31] J. R. Lakowicz, *Principles of Fluorescence Spectroscopy* Springer 2006, 3rd edition
- [32] B. Valeur “Molecular fluorescence: Principles and Applications”, 2001, Wiley-VCH
- [33] M. Lebalental, N. Djellali, C. Arnaud, J.-S. Lauret, J. Zyss, R. Dubertrand, C. Schmit, and E. Bogomolny, Phys. Rev. A **76** 023830 (2007).
- [34] H. Rabbani-Haghighi, S. Forget, S. Chénais, A. Siove, M.-C. Castex, and E. Ishow, Appl. Phys. Lett. , **95**, 033305 (2009).
- [35] M. Lebalental, E. Bogomolny, and J. Zyss, Organic micro-lasers: a new avenue onto wave chaos physics, in [36].
- [36] *Practical applications of micro-resonators in optics and photonics*, edited by A. Matsko (CRC, Boca Raton, 2009).
- [37] S. Lozenko, N. Djellali, I. Gozhyk, C. Delezoide, J. Lautru, C. Ulysse, J. Zyss, and M. Lebalental, J. Appl. Phys. **111**, 103116 (2012).
- [38] O.I. Yaroshenko, J. Opt. A, **5**, 328 (2003).
- [39] K. C. Rezyer, L. W. Casperson, J. Appl. Phys. **51**, 6075 (1980).
- [40] K. C. Rezyer, L. W. Casperson, J. Appl. Phys. **51**, 6083 (1980).
- [41] P. Liang, Q. Chen, S. Zhang, J. Lei, Appl. Phys. B **55**, 494 (1992).
- [42] I. Gozhyk, S. Forget, S. Chénais, C. Ulysse, A. Brosseau, R. Méallet-Renault, G. Clavier, R. Pansu, J. Zyss, M. Lebalental, Proceedings of SPIE **8258**, 82580K (2012).
- [43] D. Wright, E. Brasselet, J. Zyss, G. Langer, W. Kern, J. Opt. Soc. Am. B, **21**, 944 (2004).
- [44] P. Selenyi, Phys. Rev., **56**, 477 (1939).
- [45] Lee W. Casperson, W. J. Sandle, A. C. Wilson, D. M. Warrington, and R. J. Ballagh, J. Appl. Phys. **69**, 8005 (1991).
- [46] V. Le Floch, S. Brasselet, J.-F. Roch, and J. Zyss, J. Phys. Chem. B **107**, 12403 (2003).
- [47] E. Bogomolny, N. Djellali, R. Dubertrand, I. Gozhyk, M. Lebalental, C. Schmit, C. Ulysse, J. Zyss, Phys. Rev. E **83**, 036208 (2011).
- [48] V. Baev, T. Latz, P. Toschek, Applied Physics B, **69**, 171 (1999).
- [49] M. M. Mazumder, G. Chen, P. J. Kindlmann, R. K. Chang, J. B. Gillespie, Opt. Lett. **20**, 1668 (1995).
- [50] H. Taniguchi, H. Tomisawa, Opt. Lett. **22**, 1852 (1994).
- [51] S. L. Bondarev, V. N. Knyukshto, V. I. Stepuro, A. P. Stupak, A. A. Turban, J. Appl. Spectrosc., **71**, 194 (2004).
- [52] J.A.E. Wasey, , A. Safonov, I.D.W. Samuel, W.L. Barnes, Opt. Commun. **185**, 109 (2000).
- [53] The lowest theoretical limit of the electrically-driven threshold in organic semiconductor material (estimated from the value of its optically-pumped threshold under assumption of maximum recombination rate and neglecting the current-induced losses and metal contact[16]) is about 80 A/cm<sup>2</sup>[15] (as the lowest reported threshold



under optical pumping is of the order of  $100 \text{ W/cm}^2$ , reached in conjugated polymers [17]).

- [54] All the dyes were purchased from Exciton.
- [55] Gain values in dB (g[dB]) represent an overall sample amplification and may be recalculated to  $\text{g[cm}^{-1}\text{]}$  using expression  $10^{g[\text{dB}]/10}/l[\text{cm}]$ , where  $l$  [cm] is the sample length in cm.
- [56] PMMA stands for poly(methylmetacrylate). For pump-probe measurements, the layer must be thick. So we used a molecular weight of 950.000 and a concentration of 15 wt% in anisole (MicroChem). For all other experiments described in this article, the molecular weight of PMMA is 495.000 and the concentration is 6 wt% in anisole (MicroChem).
- [57] To optimize the absorption of the pump beam through the whole thickness of the layer, the concentration of DCM was set to 1.4 wt% . But for all other experiments described in this article, the concentration of DCM is 5 wt%.
- [58] The sizes of the beams correspond to the full width at half maximum and were measured with an imaging system.
- [59] With the parameters of this experiment, the correction corresponds to the absorption of the pump over an effective thickness  $h_{eff} = 9 \text{ }\mu\text{m}$ , ie. half the actual layer thickness.
- [60] Error in Eq. (6) of [42]. It should be read  $\cos 2\varphi \cos 2\alpha$  instead of  $\cos(2\varphi + 2\alpha)$